Fuel 316 (2022) 123339

Contents lists available at ScienceDirect

Fuel

journal homepage: www.elsevier.com/locate/fuel

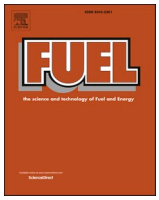

Full Length Article

Study on particle loss in high-temperature flue gas sampling during fuel conversion

Zuozhou Tang, Bingqiang Ji *, Zhongwei Li, Qiang Song *

Department of Energy and Power Engineering, Tsinghua University, 100084 Beijing, China

ARTICLE INFO

Keywords:
Particle
Flue gas sampling
Thermophoresis
Deposition rate

ABSTRACT

The sampling accuracy for high-temperature flue gas is limited by the particle deposition on the sampling tube wall, which is important for the study of fuel conversion. Herein, deposition of 0.1–10 μm particles in 300–1000 K flue gas in the sampling tube is numerically investigated, and the corresponding particle loss is quantified by theoretical modeling. Saffman lift force and thermophoretic force dominate the particle deposition in the isothermal and cooling sections of the tube, respectively. Along the tube, the cumulative deposition rate is negligible in the isothermal section and increases rapidly and then gradually reaches the terminal deposition rate in the cooling section. The terminal deposition rate increases with the flue gas temperature, which can be up to 40.77% and 24.62% for 0.1 μm and 10 μm particles in 1000 K flue gas, respectively. A formula of the terminal deposition rate is proposed as a function of the flue gas temperature, which predicts the numerical results with an error less than 5%. The normalized profiles of the cumulative deposition rate under different sampling condition coincide, and a distribution function related to the flow Reynolds number is proposed. Based on the above formula and function, a model is presented which well predict the particle loss in the sampling tube with different lengths.

1. Introduction

Sampling and characterizing the products is an essential experimental method to study the thermochemical processes. High-temperature flue gas sampling is often applied in the research on fuel thermochemical conversion [1–3]. The solid products, i.e., the small particles, in the flue gas are withdrawn isokinetically from the source and collected by the filter, or size-segregated by the impactors such as the Electrical Low Pressure Impactor [4–6]. If the reactions continue or condensation and nucleation occur in the sampling tube, the size distribution of the particles will change and the dilution sampling is suggested [6–8]. However, this method is not widely used in small-scale benches owing to its complexity and large space requirements. During high-temperature flue gas sampling, it was found that the particles in the sample gas deposit on the wall of the sampling tube, resulting in a significant sampling loss [9–11] and deterioration of the sampling recovery. Moreover, the sampling loss might vary with the particle size, which misleads the understanding of fuel conversion.

Large particles (>10 μm) would deviate from the streamline and deposit due to gravity and at the elbow area due to the inertia [12]. As the particle size decreases, the effects of gravity and inertia decrease rapidly [13]. In the sampling tube with obvious temperature and velocity gradients, PM_{10} moves under forces mainly including drag force, Brownian, thermophoresis, and Saffman lift forces [14]. The drag and Brownian forces affect more obviously on small particles, while the Saffman lift force is more significant in the high velocity gradient region [15,16]. The thermophoretic force yielded by the large temperature gradient drives suspended particles to migrate toward the cold tube during the high-temperature sampling [17,18]. Previous studies on the particle's motion between parallel plates or around a sphere showed that the thermophoresis deposition increases with the temperature gradient [19,20]. The experiments by Nishio et al. [21] reported deposition rates of 3% and 5% of the polydispersed particles when the temperature differences are ~ 50 K and ~ 100 K in a cooling tube of 1 m in length and 5 mm in diameter, respectively. In a tube of 0.965 m in length and 4.9 mm in diameter with a wall temperature of 293 K, Romay et al. [22] found that the deposition rate ranges from 7.2% to 12.7% and 4.6 % to 7.0 % when the gas temperature ranges from 349.0 K to 418.2 K for 0.1 μm particles and 336.5 K to 365.8 K for 0.482 μm particles, respectively. Experimental and numerical studies also found that smaller particles suffer from a more obvious thermophoretic effect and thus move faster

* Corresponding authors.
E-mail addresses: bingqiangj@163.com (B. Ji), qsong@tsinghua.edu.cn (Q. Song).

https://doi.org/10.1016/j.fuel.2022.123339
Received 22 September 2021; Received in revised form 9 December 2021; Accepted 16 January 2022
Available online 22 January 2022

Nomenclature

c_p	specific heat of sample gas, J·kg^{-1}·K^{-1}
C	number concentration of particles, m^{-3}
C_c	Stokes-Cunningham slip correction
d_p	diameter of the particle, m
D	diameter of tube, m
$\boldsymbol{F}_D$	drag force, N
$\boldsymbol{F}_S$	Saffman lift force, N
$\boldsymbol{F}_T$	thermophoretic force, N
h	enthalpy of sample gas, J·kg^{-1}
I	identity matrix
k	thermal conductivity, W·m^{-1}·K^{-1}
K	thermophoresis coefficient
L_1	length of the isothermal section, m
L_2	length of the cooling section, m
m_p	mass of the particle, kg
p	pressure, Pa
Pr	Prandtl number of the gas
Q_{in}	flow rate, m^3·s^{-1}
r	radial position, m
Re	Reynolds number
T	temperature, K
T_c	ambient temperature, K
T_e	average sample gas temperature of the cooling process, K
T_{iso}	wall temperature of the isothermal section, K
$\boldsymbol{u}$	velocity vector of the particle, m·s^{-1}
$\boldsymbol{v}$	velocity vector of the sample gas, m·s^{-1}
z	axial position, m
α	thermal diffusivity of the sample gas, m^2·s^{-1}
η_c	cumulative deposition rate
η_t	terminal deposition rate
λ	molecular mean free path of the sample gas, m
μ	dynamic viscosity, Pa·s
ρ	density, kg·m^{-3}

Subscripts

g	sample gas
in	inlet
p	particle
wall	at the wall surface
z	in the z-direction

under the same temperature gradient [19,20,22]. However, existing experimental studies on the thermophoretic deposition of particles in the tube mainly focused on the conditions where the temperature difference is less than 200 K. Because of the much higher temperature difference, the particle loss under different particle sizes and sampling parameters in the high-temperature flue gas sampling need to be quantified.

Several correlations regarding the thermophoretic deposition rate of particles in the cooling tube have been proposed. Walker et al. [23] numerically calculated the distribution of particles in the tube and proposed a fitting formula for the overall deposition rate. Batchelor and Shen [24] found the formula by Walker et al. [23] is a special case when the temperature and particle concentration distributions are proportional, and further proposed a correction for conditions when these two fields are decoupled, where the thermophoretic deposition rate is a function of *PrK* (*Pr* is the Prandtl number of the gas and *K* is the thermophoresis coefficient) and the dimensionless temperature. Based on these two parameters, several empirical formulas in different forms were proposed by fitting numerical results, and the accuracies have been verified by experiments with temperature differences lower than 200 K [25,26]. In these studies, the ambient temperature was selected to calculate the gas and particle properties and *PrK*. However, the corresponding gas properties (as well as *PrK* and the deposition rate) in high-temperature flue gas sampling are significantly different from that in the ambient temperature and varies along the sampling tube due to the continuously decreasing gas temperature. Thus, it is necessary to consider the changes in the gas properties and propose an accurate method to predict the thermophoretic deposition rate. Furthermore, in the high-temperature sampling, the flow field and the temperature field in the tube change significantly as the flue gas temperature decreases due to the cooling effect of the tube wall. In this condition, the effects of other deposition mechanisms causing the particle loss still need to be investigated.

To evaluate the particle loss in high-temperature flue gas sampling and illustrate the corresponding particle deposition mechanism, this study numerically investigates the flue gas flow, heat transfer, and particle motion in a sampling tube. The movement and deposition behavior of 0.1–10 μm particles in 300–1000 K flue gas are analyzed. The terminal and cumulative deposition rates are calculated and the influences of different sampling parameters are discussed. Finally, theoretical formulas are proposed to predict the particle deposition rate in the high-temperature flue gas sampling tube under different sampling conditions.

2. Governing equations and numerical method

A circular tube with a diameter of D and length of $L_1 + L_2$ for sampling the high-temperature flue gas in the furnace is considered, as shown in Fig. 1, where z and r indicate the axial and radial coordinates, respectively. During sampling, part of the sampling tube, namely, the isothermal section, is located in the high-temperature flue gas sampling area (with a length of $L_1 = 0.5$ m). The flow in this section is isothermal because the wall temperature T_{iso} is the same as the sampling temperature T_{in} in the furnace. The other part of the sampling tube, namely, the cooling section, is located outside the furnace (with a length of $L_2 = 2.0$ m). The wall temperature is approximately the same as the ambient temperature T_c. The flue gas with temperature T_{in} and flow rate Q_{in} enters the sampling tube from the left inlet and exits from the right outlet. The particles are uniformly distributed at the inlet section. After experiencing different trajectories, some particles migrate to the wall of the tube and deposit, and the remaining particles escape from the outlet.

2.1. Equations of fluid flow

The sample gas is regarded as an ideal gas. In general sampling equipment, $Q_{in} \leq 10$ L·min^{-1} and $D \geq 10$ mm, yielding a Reynolds number, $Re = 4\rho_g Q_{in}/\pi\mu_g D$ less than 1500 for general flue gas with a temperature lower than 1000 K, where ρ_g and μ_g are the density and dynamic viscosity of the gas, respectively. Thus, the flow in the tube is laminar and steady during the sampling. The continuity, momentum conservation, and energy conservation equations of the gas flow in the tube are as following.

$$\nabla\cdot(\rho_g \boldsymbol{v}) = 0 \tag{1}$$

$$\nabla\cdot(\rho_g \boldsymbol{v}\boldsymbol{v}) = -\nabla p + \nabla\cdot\left[\mu_g\left(\nabla\boldsymbol{v} + \nabla\boldsymbol{v}^T - \frac{2}{3}\nabla\cdot\boldsymbol{v}I\right)\right] \tag{2}$$

$$\nabla\cdot\left[\boldsymbol{v}\rho_g\left(h + \frac{v^2}{2}\right)\right] = \nabla\cdot(k_g\nabla T_g) \tag{3}$$

where $\boldsymbol{v}$ is the velocity vector of the gas, p is the pressure, I represents the identity matrix, k_g is the thermal conductivity of the gas, and h is the

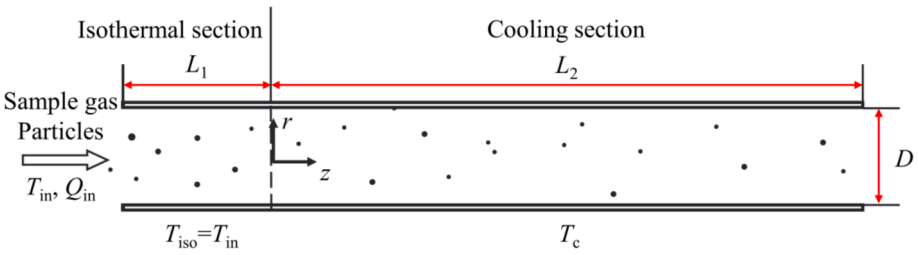

Fig. 1. Sketch of the sampling tube.

enthalpy of the gas of temperature T_g, which can be calculated as

$$h = \int_{T_{ref}}^{T_g} c_p \mathrm{d}T \tag{4}$$

where c_p is the specific heat of gas, and the reference temperature $T_{ref} = 298.15$ K.

2.2. Equations of particle motions

In general, the volume fraction of particles in a sampling flue gas is less than 0.001. Thus, the particle phase can be set as a discrete phase, and its effect on the gas flow can be neglected [27]. Moreover, the collision and aggregation between particles can be ignored. The particle is assumed to be spherical, and the motion equation of the particle is obtained from Newton's second law,

$$m_p \frac{\mathrm{d}\boldsymbol{u}}{\mathrm{d}t} = \boldsymbol{F}_D + \boldsymbol{F}_T + \boldsymbol{F}_S + \boldsymbol{F}_B \tag{5}$$

where $m_p = \rho_p \pi {d_p}^3/6$ is the mass of the particle, ρ_p and d_p are the density and diameter of the particle, respectively, and $\boldsymbol{u}$ is the velocity vector of the particle. The four terms on the right side of Eq. (5) represent the drag force, thermophoretic force, Saffman lift force, and Brownian force. The gravity is not included in Eq. (5) due to its negligible value in comparison for particles with $d_p = 0.1$–10 μm. The drag force is obtained as follows [28],

$$\boldsymbol{F}_D = -\frac{3\pi\mu_g d_p(\boldsymbol{u}-\boldsymbol{v})}{C_c} \tag{6}$$

where C_c is the Stokes-Cunningham slip correction [28],

$$C_c = 1 + \frac{2\lambda}{d_p}\left(1.257 + 0.4\mathrm{e}^{-1.1 d_p/2\lambda}\right) \tag{7}$$

where $\lambda = \mu_g/p \cdot \sqrt{\pi R T_g/2M}$ is the molecular mean free path of the gas. $R = 8.134$ J·mol^{-1}·K^{-1} is the universal gas constant, and $M = 28.966$ g·mol^{-1} is the molar mass of the sample gas.

The thermophoretic force $\boldsymbol{F}_T$ can be calculated using the model proposed by Talbot et al. [29],

$$\boldsymbol{F}_T = -\frac{3\pi d_p \mu_g^2 K}{\rho_g C_c}\frac{\nabla T_g}{T_g} \tag{8}$$

where K is the thermophoresis coefficient [30],

$$K = \frac{2C_c C_s\left(\frac{k_g}{k_p} + C_t\frac{2\lambda}{d_p}\right)}{\left(1 + 3C_m\frac{2\lambda}{d_p}\right)\left(1 + \frac{2k_g}{k_p} + C_t\frac{4\lambda}{d_p}\right)} \tag{9}$$

where $C_s = 1.17$, $C_m = 1.14$, and $C_t = 2.18$. k_p is the thermal conductivity of the particles.

The Saffman lift force in the r-direction has been defined by Saffman [15] and Asmolov [31] as

$$F_{S,r} = 0.25 C d_p^2 (v_z - u_z)\left(\mu_g \rho_g \partial v_z/\partial r\right)^{0.5} \tag{10}$$

In general, $C = 6.46$. v_z and u_z are the velocities of the gas and particle in the z-direction, respectively. The Brownian force $\boldsymbol{F_B}$ is modeled as a Gaussian white noise random process [32].

2.3. Numerical methods

A two-dimensional axisymmetric domain is adopted considering the laminar flow, and the mesh is structured with the grids refined within the boundary layer involving notable velocity and temperature gradients. A grid number of 7.30×10^5 is adopted after the independence analysis.

The commercial computational fluid dynamics software ANSYS FLUENT V14.5 is used to perform the simulation. The distributions of the flue gas flow and temperature fields are evaluated using a pressure-based solver. The SIMPLE algorithm is used to solve the pressure–velocity coupling equation. The second-order scheme is adopted for pressure discretization and the second-order upwind scheme is adopted for momentum and energy discretization. The discrete phase model (DPM) is used to calculate the particle motion. The equation of particle motion is incorporated with a user-defined function.

The dynamic viscosity μ_g, specific heat c_p, and thermal conductivity k_g of the gas are calculated using fitting polynomials as a function of the gas temperature [33]. The parameters of fly ash particles in power plants are selected as the particulate matter parameters [34] with $\rho_p = 1550$ kg·m^{-3}, $k_p = 0.33$ W·m^{-1}·K^{-1}, and $d_p = 0.1$–10 μm. The tube wall is set as no-slip. By comparing the simulated impact velocity with the critical sticking velocity of silica particles which has similar physical properties of fly ash, it is assumed that all the particles deposit after colliding with the wall [35]. The inlet and outlet of the tube are set as velocity inlet and outflow, respectively. Considering the requirement in isokinetic sampling that the sampling probe is perpendicular to the direction of the gas flow direction, the particles enter the sampling tube at a uniform axial velocity which is the same as the gas velocity.

In the simulation, particles with a total number of N_t are uniformly distributed along $r = 0$-$D/2$ at the inlet. The cumulative deposition rate η_c at an axial position z is calculated as

$$\eta_c(z) = 1 - \left(\frac{N_t - N_d(z)}{N_t}\right)^2 \tag{11}$$

where N_d is the number of particles deposited on the wall between $-L_1$ and z; N_t is set to be 5000 after the independence analysis. In this study, the gas at the outlet of the tube attains thermal equilibrium with the wall, and the overall deposition rate will not increase when further increasing the tube length. Thus, the overall deposition rate when $z = L_2$ is the terminal deposition rate η_t in a tube with infinite length.

The terminal deposition rates η_t in a circular water-cooled (T_c = 20℃) tube at different sampling temperatures T_{in} are calculated numerically and compared with the experiments conducted by Romay et al. [22], as shown in Fig. 2. The numerical results agree with the experimental results well, indicating that the numerical methods and settings adopted in this study can accurately describe the actual sampling process.

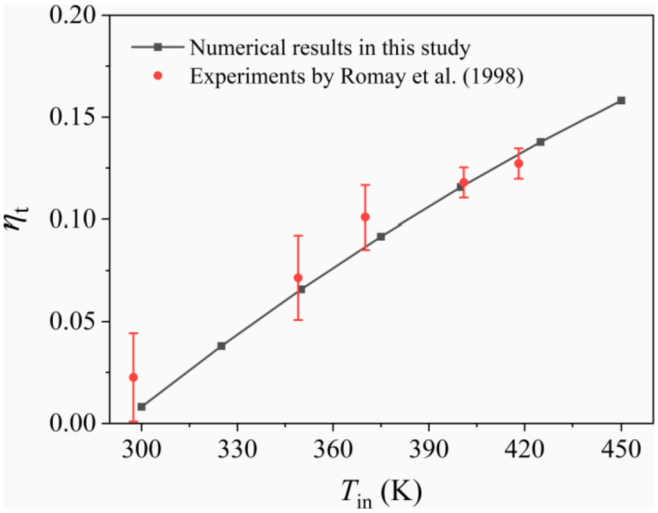

Fig. 2. Model validation by comparing the terminal deposition rates η_t at different sampling temperature T_{in} calculated numerically with that obtained by the previous experiment [22].

3. Results and discussion

3.1. Movement and deposition of particles in the sampling tube

The flow and temperature fields determine the forces acting on the particles, thereby influencing the movement and deposition behavior of the particles. Taking the operation condition with $Q_{in} = 5$ L·min^{-1}, $T_{in} =$ 600 K, $T_c = 300$ K, and $D = 10$ mm as an example, the movement and deposition behavior of 8 μm and 0.1 μm particles are analyzed to show the behaviors of micron and submicron particles in the sampling tube, respectively.

Fig. 3(a) shows the velocity $\boldsymbol{v}$ and temperature T_g distributions of the gas in the sampling tube. Owing to the viscous shear stress near the wall, the velocity distribution of the gas becomes uneven rapidly after entering the tube and gradually becomes fully developed after approximately 0.3 m in the isothermal section. In the cooling section, the gas velocity continuously decreases because of the increase in the gas density caused by the decreasing gas temperature, especially between $z =$ 0 and 0.4 m where the average gas temperatures decrease from 600 K to 343.94 K. Fig. 3(b) shows the distribution of the velocity gradient -dv_z/dr near the entrance within the red dashed rectangle in Fig. 3(a). The radial gradient of the axial velocity in this area is the maximum owing to the rapid change in the velocity, reaching up to 9.56×10^4 s^{-1}. The thickness of the velocity boundary layer increases while the velocity gradient decreases along the tube. Furthermore, Fig. 3(b) shows the streamlines near the tube wall of the inlet, where the gas flows toward the center of the tube owing to the thickening of the velocity boundary layer. Fig. 3(c) shows the distribution of the gas temperature gradient ∇T_g along the radial position r at different axial positions between $z =$ 0 and 0.4 m within the blue dashed rectangle in Fig. 3(a). The closer to the wall, the larger the temperature gradient. The maximum temperature gradient decreases from 2.11×10^5 K/m to 5.80×10^4 K/m from z = 0.02 m to $z = 0.2$ m. The temperature boundary layer gradually thickens but the temperature gradient in the temperature boundary layer decreases along the tube.

Fig. 4 shows the trajectories of 8 μm particles colored by the particle velocity departing from different radial positions. In Fig. 4(a), particles 1–3 depart from $r_{in} = 4.995$ mm, 4.99 mm, and 4.985 mm, respectively. These particles tend to move toward the center of the tube first under the action of drag force and then toward the wall under the action of the Saffman lift force considering the large velocity gradient shown in Fig. 3 (b). Particles 1 and 2 deposit on the wall of the isothermal section, while particle 3 escapes from the isothermal section and rapidly migrates toward the wall and deposits in the cooling section. Particles 4–6 departing from $r_{in} = 4.860$ mm, 4.660 mm, and 4.460 mm move toward the center of the tube under the action of drag force in the isothermal section and migrate toward the wall in the cooling section, as shown in

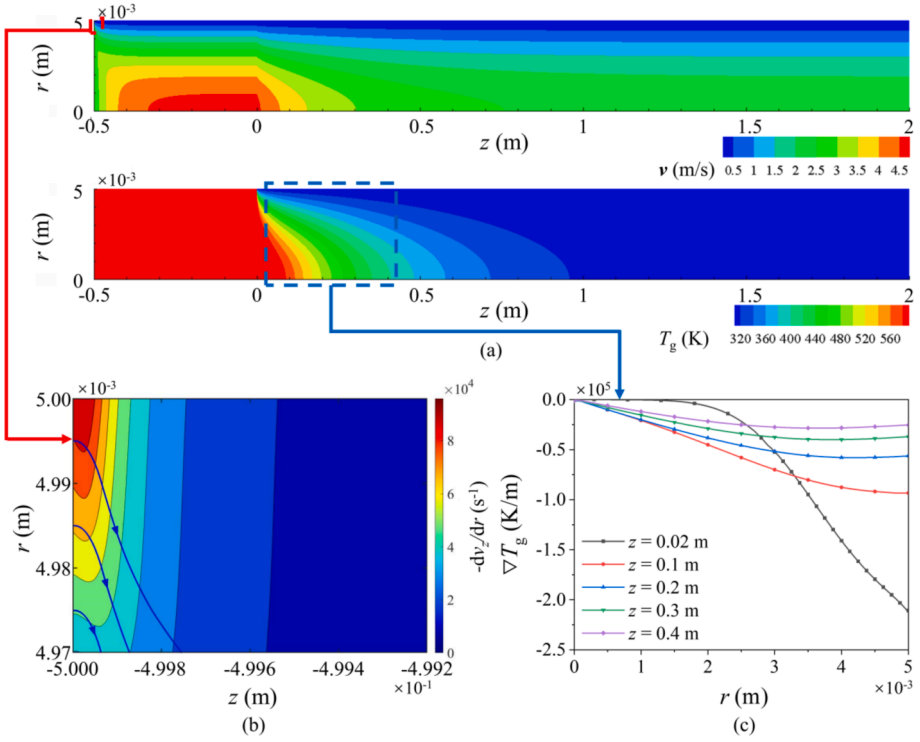

Fig. 3. (a) Distributions of the gas velocity $\boldsymbol{v}$ and temperature T_g in the tube, (b) distributions of the radial gradient of gas velocity -dv_z/dr and streamlines near the wall in the entrance area, (c) distributions of the radial gradient of gas temperature ∇T_g at different z in the cooling section.

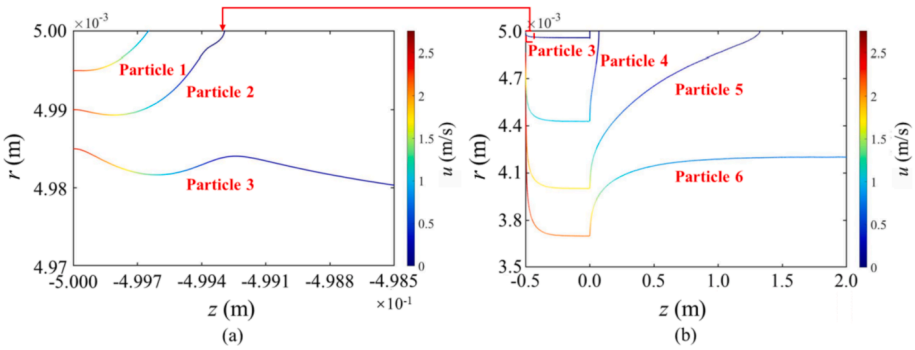

Fig. 4. Trajectories of 8 μm particles departing from different radial positions in (a) the isothermal section and (b) the whole tube.

Fig. 4(b). The overall trajectory and deposition position of the particle tend to shift upstream when the departure position is nearer the center of the tube. Particles 3–5 finally deposit in the cooling section while particle 6 escapes from the tube. The Saffman lift force promotes the deposition of 8 μm particles when the departure position is very near to the tube wall ($r_{in} \geq 4.990$ mm) and drives the radial motion of other particles toward the wall. Most of the deposited particles (4.899 mm $\geq r_{in} \geq$ 4.657 mm) deposit on the wall in the cooling section under the thermophoretic force, which is thus the dominant force for the deposition of micron particles.

Fig. 5 shows the trajectories of 0.1 μm particles departing from different radial positions colored by the particle velocity. In Fig. 5(a), particles 7–9, with the same departure positions as particles 1–3 (r_{in} = 4.995 mm, 4.99 mm, and 4.985 mm) respectively, do not migrate toward the wall in the isothermal section and enter the cooling section. This is due to the much smaller Saffman lift force comparing to the drag force for 0.1 μm particles since the Saffman lift force is proportional to d_p^2 and the velocity difference v_z-u_z which is small for 0.1 μm particles. In Fig. 5(b), particles 7–9 rapidly migrate toward the wall and deposit. Departing from r_{in} = 4.5 mm, 4.25 mm, 4.25 mm, and 4.0 mm respectively, particles 10–13 migrate toward the center of the tube in the isothermal section and move toward the wall in the cooling section under the action of thermophoresis, similar to the trajectories of particles 4–6. Finally, particle 10 deposits while particle 13 escapes from the tube owing to the farther departure distance from the wall. Particle 11 deposits while particle 12 escapes because the Brownian motion of the particles introduces uncertainties in the trajectory and deposition behavior of the particles departing from the same position. The Brownian force exerts more effect on the motion of 0.1 μm particles than that of 8 μm particles. The simulation also indicates that the Brownian force does not influence the statistical results of the deposition rate for the particles in this study. There is no deposition when the thermophoresis is not considered in the simulation, indicating that thermophoresis is the dominant mechanism for the deposition of submicron particles in the sampling tube.

3.2. Effects of sampling parameters on the deposition rate

Based on the mechanism of particle deposition in the high-temperature sampling tube discussed in Section 3.1, the influences of sampling parameters including the sampling temperature, gas flow rate, and the tube diameter on the deposition rate of particles in the sampling tube are examined here.

Fig. 6 shows the terminal deposition rate η_t of 0.1–10 μm particles at different sampling temperatures T_{in} when Q_{in} = 5 L/min, T_c = 300 K, and D = 10 mm. In general, η_t decreases with the increase in particle diameter. When the sampling temperature is 1000 K, η_t of the 0.1, 1, 10

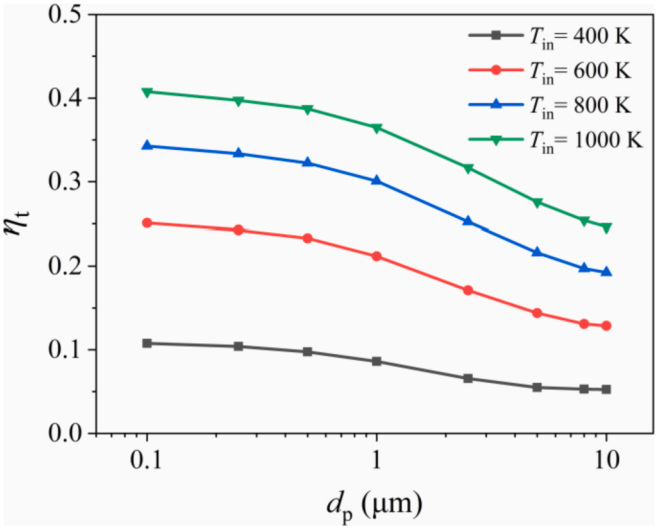

Fig. 6. The terminal deposition rate η_t of particles with different diameters d_p in the tube under different sampling temperatures T_{in}. Here, Q_{in} = 5 L/min, T_c = 300 K, D = 10 mm.

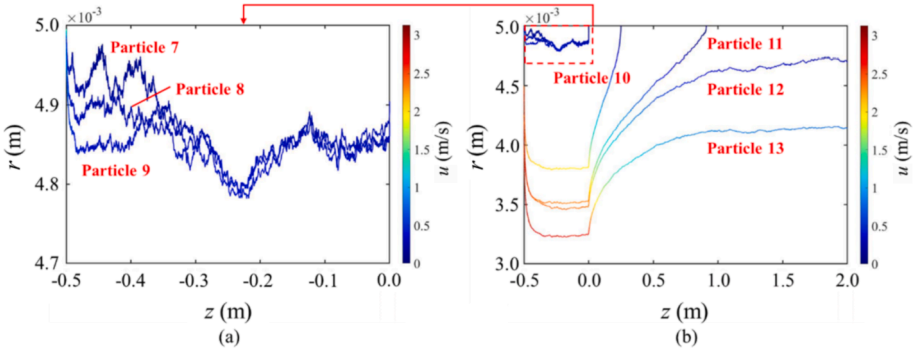

Fig. 5. Trajectories of 0.1 μm particles with different departure radial positions in (a) the isothermal section and (b) the whole tube.

μm particles in the tube are 40.77%, 36.48%, and 24.62%, respectively. Thus, the deposition of 0.1–10 μm particles cannot be neglected for high-temperature sampling. η_t of submicron particles decreases slightly, whereas that of micron particles decreases significantly with the increase in particle size. This is because the importance of the dominant force of particle deposition, i.e., the thermophoretic force, decreases with particle size in comparison to the drag force. For particles of the same diameter, the terminal deposition rate increases as the sampling temperature increases, due to the larger thermophoretic force under a larger temperature gradient.

Fig. 7(a-c) shows the axial distributions of the cumulative deposition rate η_c of three different-sized particles at different flow rates Q_{in} when $T_{in} = 600$ K, $T_c = 300$ K, and $D = 10$ mm. Only a small portion (6.1% at most) of micron particles deposit in the isothermal section. When the particles enter the cooling section, because the sampling tube is long enough to attain thermal equilibrium at the outlet, η_c increases and gradually tends to constant as the terminal deposition rate η_t which does not change with different flow rates. The cumulative deposition rate η_c of the particles subjected to the Saffman lift force in the isothermal section increases with the flow rate while the overall proportion is small and can be ignored, and thus the thermophoresis is the dominant mechanism for the deposition of 0.1–10 μm particles in the sampling tube. Smaller particles have a higher η_c in the cooling section owing to the stronger thermophoretic force. For particles with the same diameter, the axial positions with the same η_c increases linearly with Q_{in} before η_c reaches the terminal deposition rate η_t, as shown in Fig. 7(d). In other words, particles departing from the same radial position travel an axial distance linear with Q_{in} before deposition. For example, the axial positions corresponds to $\eta_c = 22.54\%$ (and $\eta_t = 25.04\%$) for 0.1 μm particles are $z = 311$ mm, 614 mm, 934 mm, and 1240 mm at flow rates of 2.5, 5, 7.5, and 10 L/min, respectively. Fig. 8 shows that the distributions of $-\nabla T_g/T_g$ along z/Q_{in} collapse into one curve at the same r, indicating a same radial velocity as well as a same thermophoretic velocity $u_T = PrK\alpha\nabla T_g/T_g$, where α is the thermal diffusivity of the gas. Meanwhile, the axial velocity and distance traveled by the particle are linear with Q_{in}. This means the particles have the same radial velocity at the same radial position. Thus, the axial positions with the same η_c increases linearly with Q_{in}.

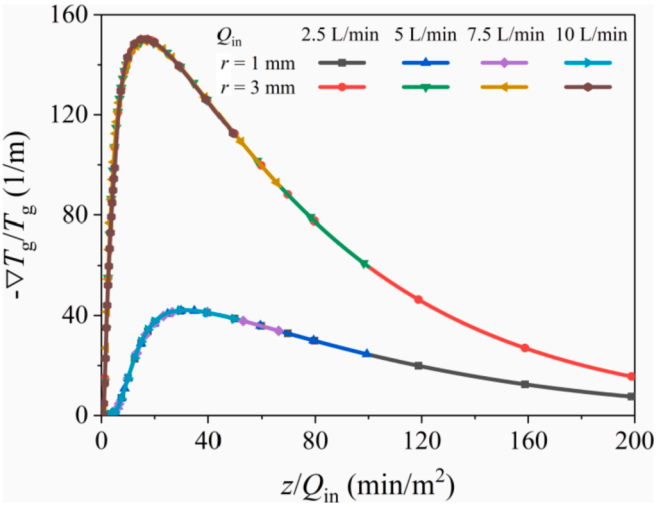

Fig. 8. Evolutions of $-\nabla T_g/T_g$ with z/Q_{in} at different radial positions r.

Fig. 9(a-c) shows the axial distributions of the cumulative deposition rate η_c of three different-sized particles at different sampling temperatures T_{in} when $Q_{in} = 5$ L/min, $T_c = 300$ K, and $D = 10$ mm. η_c of the particles subjected to the Saffman lift force near the inlet is small (≤8.03%) and negligible in comparison. Similar to the terminal deposition rate, for particles with the same diameter, η_c at the same axial position in the cooling section increases with the increase in sampling temperature due to a larger thermophoresis migration. Fig. 9(d) shows that the normalized cumulative rate η_c/η_t distributions of different-sized particles with different sampling temperatures are basically the same, indicating the axial position where η_c reaches the same percentage of η_t is consistent under the same flow rate.

Fig. 10(a) shows the distributions of the cumulative deposition rate η_c of 0.1 μm and 8 μm particles with different tube diameters D. η_c of the particles under different D does not change at a given sampling temperature and flow rate. This is because particles departing from the same dimensionless radial position $2r_{in}/D$ travel the same axial distance

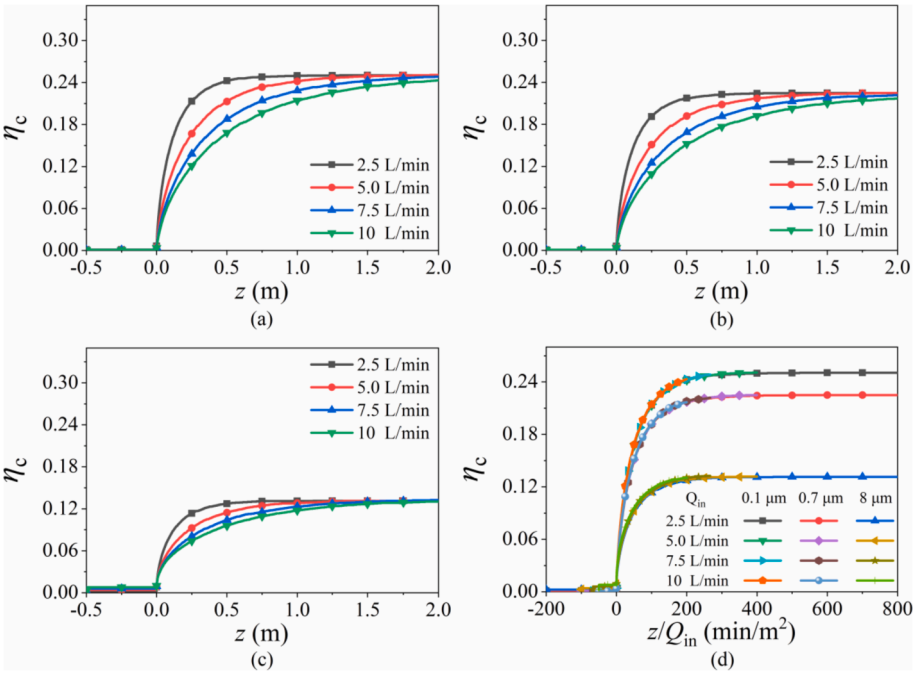

Fig. 7. Variations of the cumulative deposition rate η_c of the particles in the tube with the flow rate Q_{in} for (a) $d_p = 0.1$ μm, (b) $d_p = 0.7$ μm, and (c) $d_p = 8$ μm. (d) The cumulative deposition rate η_c as a function of z/Q_{in}. Here, $T_{in} = 600$ K, $T_c = 300$ K, and $D = 10$ mm.

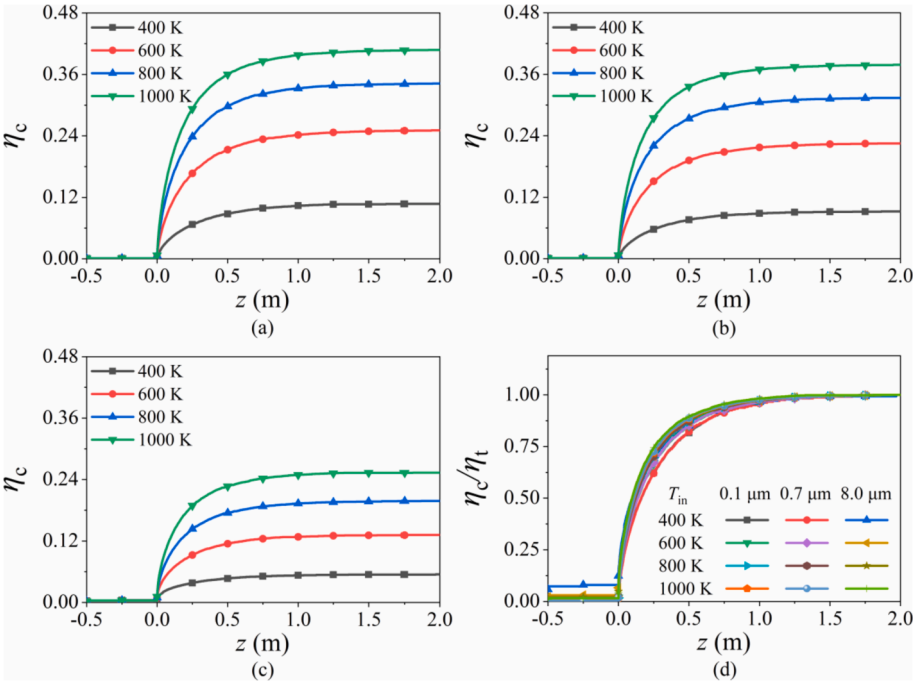

Fig. 9. Variations of the cumulative deposition rate η_c along the tube with the sampling temperature T_{in} for (a) $d_p = 0.1$ μm, (b) $d_p = 0.7$ μm, and (c) $d_p = 8$ μm. (d) The normalized cumulative deposition rate distribution along the tube. Here, $Q_{in} = 5$ L/min, $T_c = 300$ K, and $D = 10$ mm.

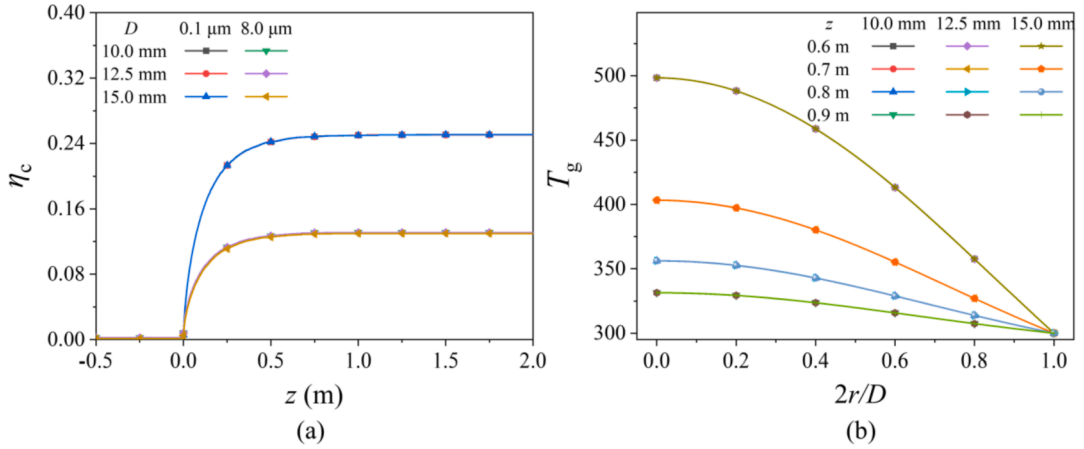

Fig. 10. (a) Variations of the cumulative deposition rate η_c along the tube under different tube diameters D. (b) The variation of the gas temperature T_g with dimensionless tube radius $2r/D$. Here, $T_{in} = 600$ K, $T_c = 300$ K, and $Q_{in} = 2.5$ L/min.

before deposition. The radial migration distance ($D/2$-r_{in}) ∝ D. The distribution of the gas temperature T_g at a given axial position remains unchanged as shown in Fig. 10(b), and thus ∇T_g as well as the thermophoretic velocity $u_T = PrK\alpha\nabla T_g/T_g$ is proportional to D^{-1}. Moreover, the particle's axial velocity $u_z \propto D^{-2}$ at the same flow rate. Therefore, the axial deposition position of the particle ($\sim(D/2\text{-}r_{in})u_z/u_T$) does not change with D.

Overall, the terminal deposition rate is only determined by the sampling temperature. The terminal deposition rates of 0.1 μm, 1 μm and 10 μm particles increases from 10.77% to 40.77%, 8.61% to 36.48% and 5.25% to 24.62% when T_g increases from 400 K to 1000 K, respectively. Higher sampling temperature and lower flow rate increase the cumulative deposition rate at the same axial position before reaching the terminal deposition rate. As a common and indispensable method in the study of thermochemical conversion processes, particle loss owing to the thermophoresis deposition in the high-temperature flue gas sampling will cause deviations in the results. Therefore, it's necessary to quantitatively predict the deposition rate in the high-temperature sampling tube.

3.3. Theoretical model for deposition rate

In this section, a method predicting the particle loss in the high-temperature flue gas sampling tube is further proposed. Since the thermophoresis dominates the deposition of 0.1–10 μm particles in the tube, the cumulative deposition rate of particles can be calculated as the ratio of the number of particles depositing on the wall under thermophoretic force in the cooling section to the total number of particles entering the tube, i.e.,

$$\eta_c(z) = \frac{\int_0^z C_{wall} u_T \cdot \pi D \mathrm{d}z}{Q_{in} C_{in}} = \frac{\int_0^z C_{wall} PrK \cdot \alpha \frac{\nabla T_{wall}}{T_{wall}} \cdot \pi D \mathrm{d}z}{Q_{in} C_{in}} \tag{12}$$

where C_{wall} is the number concentration of particles near the wall of sampling tube which varies little with the axial position; T_{wall} is the flue

gas temperature at the wall surface, $T_{wall} = T_c$; C_{in} is the particle number concentration at the inlet; $Pr = c_p\mu_g/k_g$. The corresponding gas properties are mainly dependent on the local gas temperature; K is the thermophoresis coefficient calculated by Eq. (9) which is affected by the particle diameter d_p and the properties of the particles and gas (such as the particle thermal conductivity k_p). When z is infinity, $\eta_c(z) = \eta_t$. Based on the energy conservation in the tube, we obtain

$$\int_0^{\infty} \alpha \nabla T_{wall} \cdot \pi D dz = Q_{in}(T_{in} - T_c) \tag{13}$$

According to Eqs. (12) and (13), the terminal deposition rate of particles in the tube can be expressed as

$$\eta_t = PrK \frac{T_{in} - T_c}{T_c} \frac{C_{wall}}{C_{in}} \tag{14}$$

Batchelor and Shen [24] proposed the distribution of the particle concentration in the tube as

$$\frac{C_{wall}}{C_{in}} = \frac{T_{wall}}{T_{in}} \left[1 + (1 - PrK)\left(\frac{T_{in} - T_{wall}}{T_{in}}\right)\right] \tag{15}$$

based on which Eq. (14) can be further expressed as

$$\eta_t = PrK \frac{T_{in} - T_c}{T_{in}} \left[1 + (1 - PrK)\left(\frac{T_{in} - T_c}{T_{in}}\right)\right] \tag{16}$$

The dashed line and dash-dotted line in Fig. 11(a) are the prediction results using Eq. (16) when the highest temperature T_{in} and the lowest temperature T_c in the tube are used to calculate PrK, respectively. When the temperature difference is small (e.g. $T_{in} = 400$ K), PrK is basically constant in the tube, and thus the terminal deposition rates calculated with the two temperatures are both in good agreement with the simulation results. However, when the temperature difference is large (e.g. $T_{in} = 600$–800 K), the deposition rates calculated with the two temperatures differ significantly from the simulation results. To accurately predict the deposition rate with a large temperature difference, an equivalent temperature T_e is adopted to calculate PrK in Eq. (16). By fitting the terminal deposition rate described in Fig. 6, T_e is calculated as

$$T_e = \frac{T_{in} - T_c}{lnT_{in} - lnT_c} \tag{17}$$

T_e can also be regarded as an approximation to the average gas temperature of the cooling process. The variation of the terminal deposition rate η_t with particle size d_p obtained by numerical simulation and that calculated by Eq. (16) with PrK based on T_e are shown as discrete points and solid lines in Fig. 11(a), respectively. The prediction errors are less than 5%, indicating that Eq. (16) and (17) accurately predict the terminal deposition rate of particles.

Eq. (16) and (17) show that the terminal deposition rate is determined by Pr, K, T_{in} and T_c. The flue gases with different compositions have a close Pr at the same temperature, thus Pr mainly varies with T_{in} and T_c. Considering the expression of K in Eq. (9), we can find that the key factors affecting the terminal deposition rate during flue gas sampling are particle thermal conductivities k_p, particle sizes d_p, sampling temperatures T_{in}, and ambient temperatures T_c. The influences of these four factors on the terminal deposition rate are given in Fig. 12, where the range of each factor is selected considering the practical sampling situations and the basic sampling condition is set as $k_p = 0.33$ W·m^{-1}·K^{-1}, $d_p = 2.5$ μm, $T_{in} = 600$ K, $T_c = 300$ K. Fig. 12(a) and (b) show that the terminal deposition rate decreases first fast and then slowly as the thermal conductivity k_p of the particle and the particle size d_p increases. Fig. 12(c) shows that the terminal deposition rate increases significantly as the sampling temperature T_{in} increases. Fig. 12(d) shows that the terminal deposition rate decreases nearly linearly as the ambient temperature T_c increases. No factor can be ignored, while the sampling temperature T_{in} shows the most significant influence on the terminal deposition rate.

According to Eq. (12), the normalized distribution function of the cumulative deposition rate can be obtained as

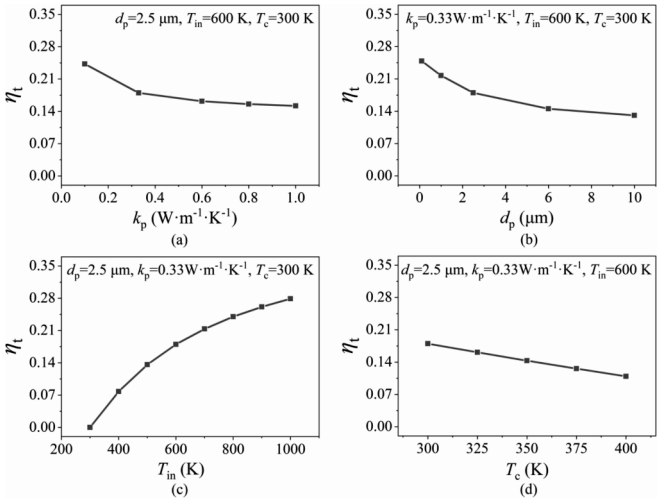

Fig. 12. Influences of thermal conductivity k_p (a), particle diameter d_p (b), sampling temperature T_{in} (c) and ambient temperature T_c (d) on the terminal deposition rate η_t.

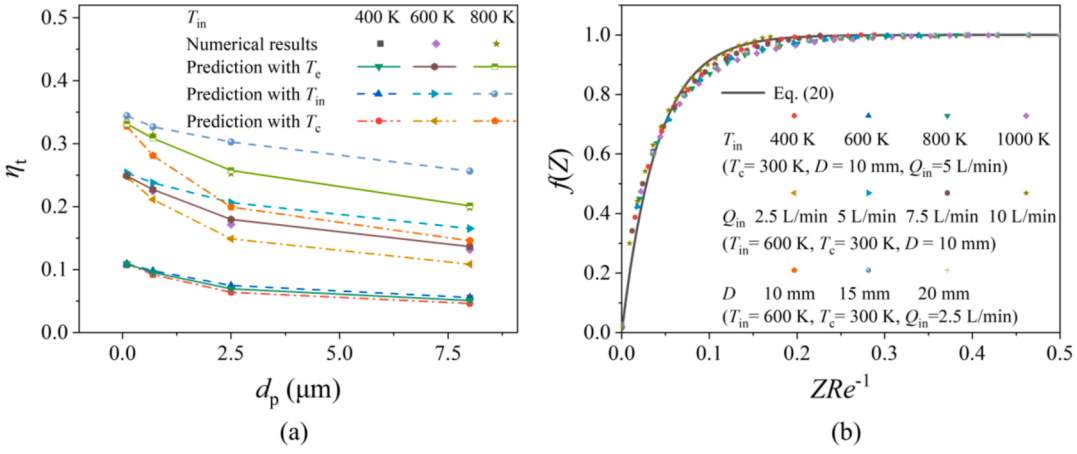

Fig. 11. Comparison between the theoretical models with the numerical simulation. (a) The terminal deposition rate η_t ($T_{in} = 400/600/800$ K, and $T_c = 300$ K) and (b) the normalized distribution function $f(z)$ of the cumulative deposition rate.

$$f(z) = \frac{\eta_c(z)}{\eta_t} = \frac{\int_0^z \nabla T_{wall} dz}{\int_0^\infty \nabla T_{wall} dz} \quad (18)$$

Considering Eq. (13), $f(z)$ can be further expressed as

$$f(z) = \left(\frac{\pi D \cdot \alpha}{Q_{in}} \frac{1}{T_{in} - T_c}\right) \int_0^z \nabla T_{wall} dz \quad (19)$$

Eq. (19) shows that $f(z)$ is only related to the integral of the wall temperature gradient. Since the fluid flow in the tube is determined by *Re*, we propose that the dimensionless normalized distribution function can be expressed as

$$f(Z) = 1 - e^{aZRe^{-1}}, Z > 0 \quad (20)$$

where $Z = z/D$ is the dimensionless axial position. The gas properties are calculated using $T = T_e$. $a = 24.53$ is obtained by fitting the numerical results in this work with a correlation coefficient $R^2 = 0.979$. $f(Z)$ calculated by Eq. (20) and obtained by numerical simulation are shown as the solid line and discrete points in Fig. 11(b), respectively. It shows that Eq. (20) predicts the cumulative deposition rate of particles along the tube well.

Thus, the cumulative deposition rate η_c at different axial positions under any sampling conditions can be predicted as

$$\eta_c(Z) = \eta_t \cdot f(Z) \quad (21)$$

4. Conclusions

The deposition behaviors of 0.1–10 μm particles in a high-temperature flue gas sampling tube are numerically studied, where the tube is divided into the isothermal section in the sampling environment and the cooling area outside the sampling environment. A large velocity gradient occurs near the wall at the entrance, yielding a Saffman lift force which drives particles to migrate toward the wall and a small portion of micron particles deposit in the isothermal section. The inlet area of the cooling section has a significant temperature gradient and thus particles migrate toward the wall under the effect of thermophoresis and deposit if the departing positions are close enough to the wall. The thermophoretic force dominates the particle deposition in the sampling tube.

Particle loss caused by thermophoretic deposition on the tube wall is significant. For example, the terminal deposition rates of 0.1 μm and 10 μm particles are 40.77% and 24.62%, respectively, with a sampling temperature of 1000 K. The terminal deposition rate decreases as the particle size increases and the sampling temperature decreases owing to a smaller thermophoresis effect. Along the sampling tube, the cumulative deposition rate is negligible in the isothermal section in comparison and gradually increases and approaches to the terminal deposition rate in the cooling section. The increases in the flow rate and particle size and the decrease in sampling temperature decrease the cumulative deposition rate before reaching the terminal deposition rate. The cumulative deposition rate distribution is unaffected by the tube diameter.

Considering the significant variation of the gas properties along the tube during high-temperature flue gas sampling, an equivalent temperature is introduced to determine the average gas properties, based on which a formula predicting the terminal deposition rate is proposed, with errors less than 5% comparing to the simulation results. Furthermore, a normalized distribution function with respect to the flow Reynolds number is introduced. Based on the combination of terminal deposition rate formula and normalized distribution function, a model is proposed which could be used to predict the particle loss well in the sampling tube with different lengths.

CRediT authorship contribution statement

Zuozhou Tang: Methodology, Software, Formal analysis, Investigation, Data curation, Writing – original draft. **Bingqiang Ji:** Validation, Formal analysis, Investigation, Writing – review & editing. **Zhongwei Li:** Methodology, Investigation. **Qiang Song:** Conceptualization, Resources, Supervision, Funding acquisition, Writing – review & editing.

Declaration of Competing Interest

The authors declare that they have no known competing financial interests or personal relationships that could have appeared to influence the work reported in this paper.

Acknowledgments

This work was supported by funds from the National Natural Science Foundation of China (51976103) and the Huaneng Group Science and Technology Research Project (HNKJ20-H50) (U20YYJC03).

References

[1] Ma P, Huang Q, Gao Qi, Li S. Effects of Na and Fe on the formation of coal-derived soot in a two-stage flat-flame burner. Fuel 2020;265:116914. https://doi.org/10.1016/j.fuel.2019.116914.
[2] Fine PM, Cass GR, Simoneit BRT. Chemical characterization of fine particle emissions from the wood stove combustion of prevalent United States tree species. Environ Eng Sci 2004;21(6):705–21.
[3] Weiland NT, Means NC, Morreale BD. Product distributions from isothermal co-pyrolysis of coal and biomass. Fuel 2012;94:563–70.
[4] Coudray N, Dieterlen A, Roth E, Trouvé G. Density measurement of fine aerosol fractions from wood combustion sources using ELPI distributions and image processing techniques. Fuel 2009;88(5):947–54.
[5] Zhuo J-K, Li S-Q, Yao Q, Song Q. The progressive formation of submicron particulate matter in a quasi one-dimensional pulverized coal combustor. Proc Combust Inst 2009;32(2):2059–66.
[6] Sui Z, Zhang Y, Yao J, Norris P, Cao Y, Pan W-P. The influence of NaCl and Na2CO3 on fine particulate emission and size distribution during coal combustion. Fuel 2016;184:718–24.
[7] Hays MD, Smith ND, Kinsey J, Dong Y, Kariher P. Polycyclic aromatic hydrocarbon size distributions in aerosols from appliances of residential wood combustion as determined by direct thermal desorption—GC/MS. J Aerosol Sci 2003;34(8):1061–84.
[8] Hildemann LM, Cass GR, Markowski GR. A dilution stack sampler for collection of organic aerosol emissions: design, characterization and field tests. Aerosol Sci Technol 1989;10(1):193–204.
[9] Gutti VR, Loyalka SK. Thermophoretic deposition in a cylindrical tube: computations and comparison with experiments. Nucl Technol 2009;166(2):121–33.
[10] Montassier N, Boulaud D, Stratmann F, Fissan H. Comparison between experimental-study and theoretical-model of thermophoretic particle deposition in laminar tube flow. J Aerosol Sci 1990;21:S85–8.
[11] Shimada M, Seto T, Okuyama K. Wall deposition of ultrafine aerosol-particles by thermophoresis in nonisothermal laminar pipe-flow of different carrier gas. Japanese Journal of Applied Physics Part 1-Regular Papers Short Notes & Review Papers 1994;33(Part 1, No. 2):1174–81.
[12] Raj Mohan B, Jain RK, Meikap BC. Comprehensive analysis for prediction of dust removal efficiency using twin-fluid atomization in a spray scrubber. Sep Purif Technol 2008;63(2):269–77.
[13] Chate DM, Kamra AK. Collection efficiencies of large water drops collecting aerosol particles of various densities. Atmos Environ 1997;31(11):1631–5.
[14] Thakurta DG, Chen M, McLaughlin JB, Kontomaris K. Thermophoretic deposition of small particles in a direct numerical simulation of turbulent channel flow. Int J Heat Mass Transf 1998;41(24):4167–82.
[15] Saffman PG. The lift on a small sphere in a slow shear. J Fluid Mech 1965;22(2):385–400.
[16] Naumov VA. Influence of Saffman's lift force on the motion of a particle in a Couette layer. J Eng Phys Thermophys (USA) 1996;68(5):683–6.
[17] De Bleecker K, Bogaerts A, Goedheer W. Role of the thermophoretic force on the transport of nanoparticles in dusty silane plasmas. Phys Rev E 2005;71(6). https://doi.org/10.1103/PhysRevE.71.066405.
[18] Li Z, Wang H. Thermophoretic force and velocity of nanoparticles in the free molecule regime. Phys Rev E 2004;70(2). https://doi.org/10.1103/PhysRevE.70.021205.
[19] Wang Ao, Song Q, Yao Q. Thermophoretic capture of submicron particles by a droplet. Atmos Environ 2016;147:157–65.
[20] Changfu Y, Guanghui Li. Direct numerical simulation of microparticle motion in channel flow with thermophoresis. J Environ Eng 2008;134(2):138–44.
[21] Nishio G, Kitani S, Takahash K. Thermophoretic deposition of aerosol-particles in a heat-exchange pipe. Ind Eng Chem Process Des Dev 1974;13(4):408–15.
[22] Romay FJ, Takagaki SS, Pui DYH, Liu BYH. Thermophoretic deposition of aerosol particles in turbulent pipe flow. J Aerosol Sci 1998;29(8):943–59.
[23] Walker KL, Homsy GM, Geyling FT. Thermophoretic deposition of small particles in laminar tube flow. J Colloid Interface Sci 1979;69(1):138–47.

[24] Batchelor GK, Shen C. Thermophoretic deposition of particles in gas flowing over cold surfaces. J Colloid Interface Sci 1985;107(1):21–37.
[25] Stratmann F, Otto E, Fissan H. Thermophoretical and diffusional particle-transport in cooled laminar tube flow. J Aerosol Sci 1994;25(7):1305–19.
[26] Tsai C-J, Lin J-S, Aggarwal SG, Chen D-R. Thermophoretic deposition of particles in laminar and turbulent tube flows. Aerosol Sci Technol 2004;38(2):131–9.
[27] Crowe CT, Schwarzkopf JD, Sommerfeld M, Tsuji Y. Multiphase flows with droplets and particles. 2nd Edition. 2012.
[28] Stokes GG. On the effect of the internal friction of fluids on the motion of pendulums. 1851.
[29] Talbot L, Cheng RK, Schefer RW, Willis DR. Thermophoresis of particles in a heated boundary-layer. J Fluid Mech 1980;101(4):737–58.
[30] Brock JR. Theory of thermal forces acting on aerosol particles. J Colloid Sci 1962; 17(8):768–1000.
[31] Asmolov ES. Motion of a suspension in the laminar boundary layer on a flat plate. Fluid Dyn (USA) 1992;27(1):49–54.
[32] Li A, Ahmadi G. Dispersion and deposition of spherical-particles from point sources in a turbulent channel flow. Aerosol Sci Technol 1992;16(4):209–26.
[33] Lemmon EW, Huber ML, Mclinden MO. NIST standard referencedatabase 23: reference fluid thermodynamic and transport properties-refprop. 9.0. NIST NSRDS - 2010.
[34] Liu J, Ji B, Tang Z, Song Q. Particle movement behavior and capture mechanism in a corrugated cooling channel. Powder Technol 2020;376:380–9.
[35] Thornton C, Ning Z. A theoretical model for the stick/bounce behaviour of adhesive, elastic-plastic spheres. Powder Technol 1998;99(2):154–62.